Supporting Information

Cation Dynamics Governed Thermal Properties of Lead Halide Perovskite Nanowires

Yuxi Wang[‡, †], *Renxing Lin*[‡, †], *Pengchen Zhu*[‡, †], *Qinghui Zheng*[‡], *Qianjin Wang*[‡], *Deyu Li*[§, *] *and Jia Zhu*[‡, *]

‡ National Laboratory of Solid State Microstructures, College of Engineering and Applied Sciences, and Collaborative Innovation Center of Advanced Microstructures, Nanjing University, Nanjing 210093, People's Republic of China

§ Department of Mechanical Engineering, Vanderbilt University, Nashville, TN 37212, U.S.A.

Corresponding Author

*E-mail: jiazhu@nju.edu.cn (Jia Zhu), deyu.li@vanderbilt.edu (Deyu Li)

Author Contributions

† These authors contributed equally to this work.

Figure S1: An SEM micrograph of a typical perovskite nanowire on the suspended device. The image was taken at a tilt angle of 45 degrees.

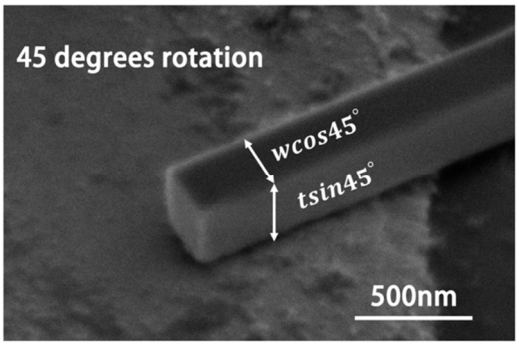

To accurately determine the thermal conductivity of perovskite nanowires, it is important to measure the rectangular cross section carefully. All the dimensions were taken in the SEM. To measure the thickness of the nanowires of rectangular cross-section, the sample was tilted to 45 degrees. Due to the typical larger than 200 nm sizes of our samples, the error from size measurement is less than 5%.

Figure S2: Selected area electron diffraction pattern of typical perovskites ((a) $CsPbBr_3$, (b) $CH_3NH_3PbBr_3$ and (c) $CH_3NH_3PbI_3$). The patterns confirm single crystalline nanowires by our growth method and high quality nanowires in thermal measurement.

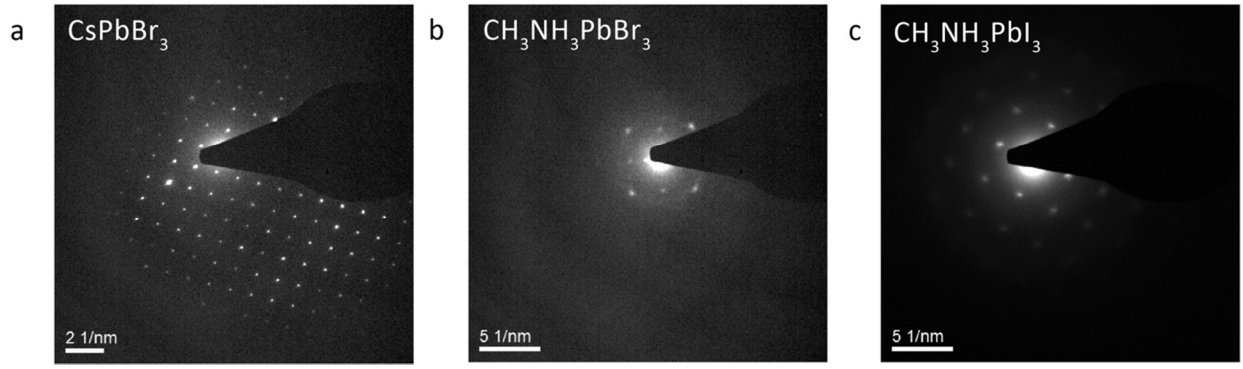

Figure S3: Thermal conductivity of other measured perovskite wires.

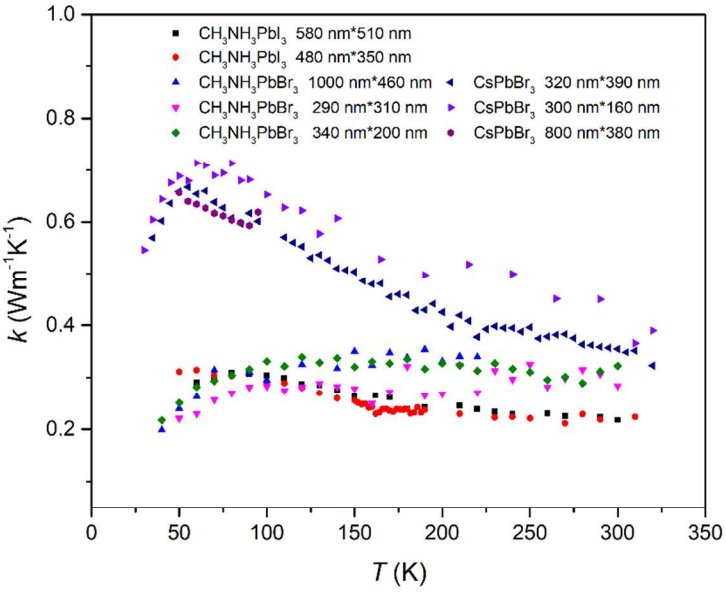

Figure S4: The measured thermal conductivity of the $MAPbI_3$ nanowire around the phase transition temperature, which indicates a dip around 160 K.

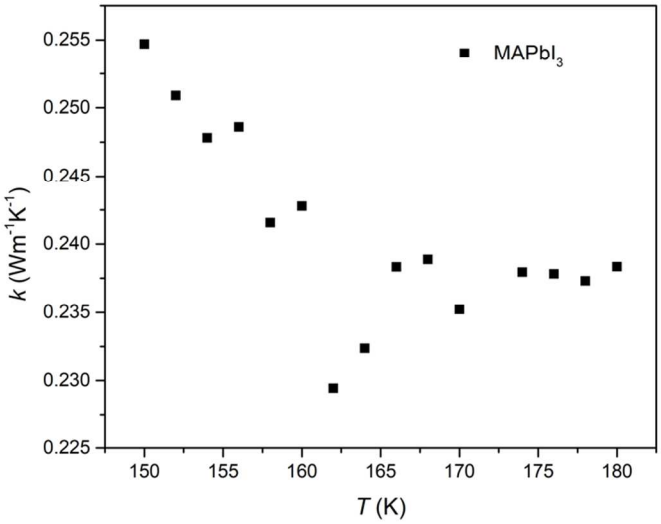

Figure S5: Sensitivity of the modelling results to the fitting parameters for orthorhombic phase $MAPbI_3$. (a), (b), (c) and (d) describe the modelling results in comparison with experimental data of $MAPbI_3$. By varying one of the modelling parameters A(a), B(b), C(c) and ω_0(d) from the best fit value with +/-10% and +/-20% deviation but leaving other three parameters unchanged, we can observe that the modelling results significantly deviate from the experimental data.

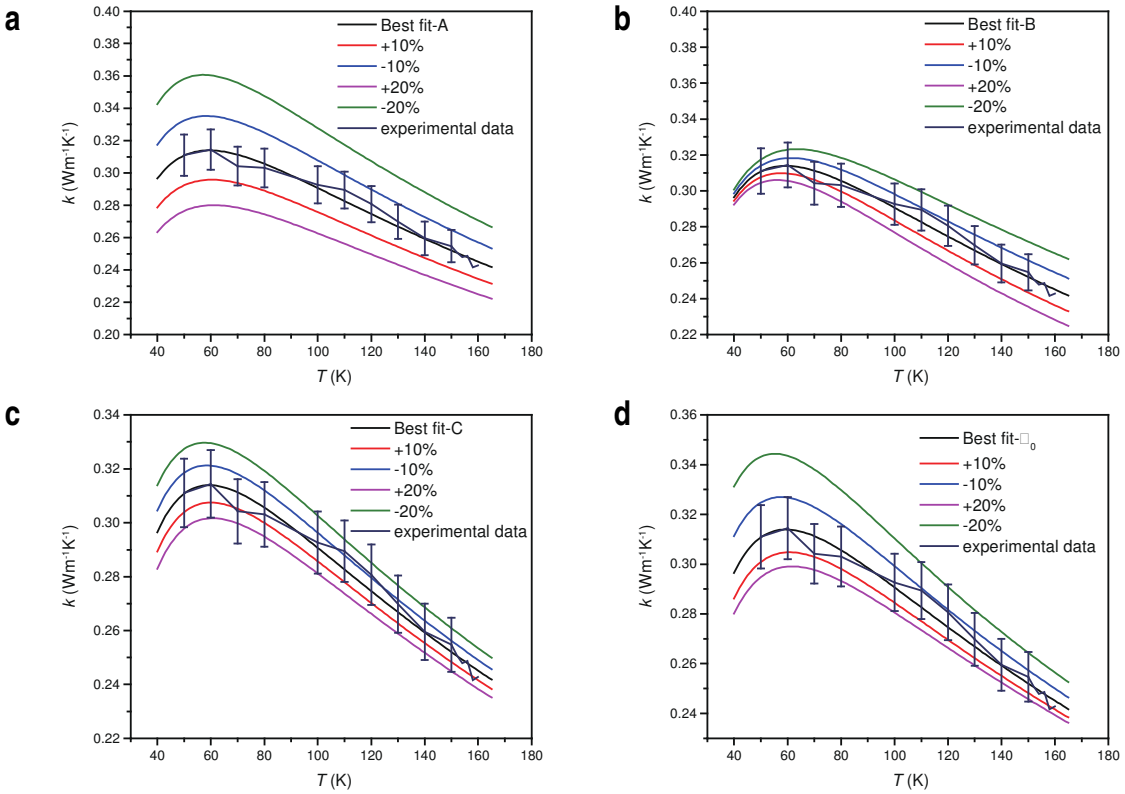

Figure S6: Absolute values of the sensitivity coefficients with respect to modelling parameters *A*, *B*, *C* and ω_0 versus temperature for orthorhombic phase $MAPbI_3$.

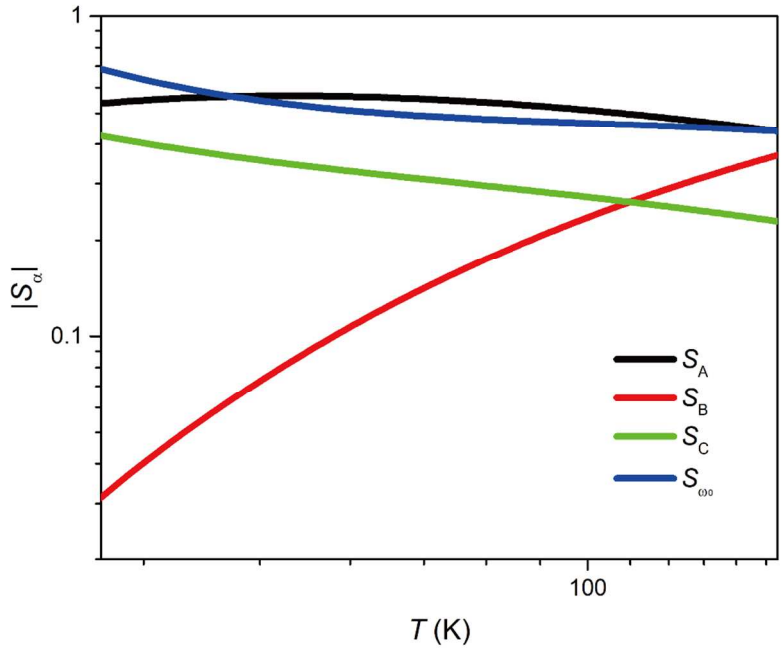

Note 1: Debye-Callaway model analysis

To demonstrate the mechanism of phonon transport in lead halide perovskites, we use the Debye-Callaway model to analyze our experimental results. The thermal conductivity *k* in the model can be expressed as,

$$k(T) = \frac{k_B}{2\pi^2 v}\left(\frac{k_B T}{\hbar}\right)^3 \int_0^{\frac{\theta}{T}} \tau \frac{x^4 e^x}{(e^x - 1)^2} dx,$$

where k_B is the Boltzmann constant, v is the speed of sound, θ is the Debye temperature, and $1/\tau$ is the phonon scattering rate based on all relevant scattering mechanisms. The phonon relaxation time τ in perovskites can usually be expressed as,

$$\tau^{-1} = \frac{v}{d} + A\omega^4 + B\omega^2 T e^{-\theta/3T} + C\frac{\omega^2 {\omega_0}^2}{(\omega^2 - {\omega_0}^2)^2},$$

where v is the speed of sound, d is the grain boundary size of the nanostructure and *A*, *B* and *C* are temperature independent fitting parameters. The four terms on the right-hand of the above expression represent boundary scattering, impurity scattering, Umklapp scattering and dynamic disorder induced scattering at low temperature, respectively.

The speed of sound and Debye temperature were adapted from the literature[1-3] and *A*, *B*, *C* and ω_0 are the four fitting parameters. v is estimated by the average sound speed of different acoustic branches.

The characteristic grain boundary size *d* is calculated from the Casimir length ($\sqrt{4wh/\pi}$, where *w* is the width and *h* is the height). All parameters for the modelling curves in Figure 3b were listed in the Table S1. We carefully adjust the four independent parameters to fit the experimental data. The modelling curves are well consistent with the analysis in the main text. The modelling parameter *C* was set to be zero for all-inorganic $CsPbBr_3$. These collectively demonstrate the effect of dynamic disorder on reducing *k* in the low temperature regime.

To confirm that the modelling results capture the transport mechanisms of hybrid perovskites at low temperatures, we need to identify the uniqueness of the model parameters. Here, for example, for orthorhombic phase $MAPbI_3$, we adjust one parameter and leave the other three fixed for several groups of modelling results, as shown in Figure S5. We can see with only +/-10% deviation from the best fit values of the modelling parameters, the modelling results deviate significantly from the best fit. For example, we found that only +/-10% deviation from the best fit value of ω_0 could result in deviations larger than the measurement uncertainties. +/-20% perturbation from the best fit of parameters would result in even larger discrepancy. These analyses also demonstrate the important role of *B* at relatively high temperature and the

important role of C and ω_0 at low temperature. Therefore, we believe that the modelling parameters given in Table S1 should reasonably reflect the phonon scattering physics in our materials systems.

In the above analyses, it is shown that the calculated thermal conductivity is sensitive to each modeling parameter. To further demonstrate the uniqueness of the fitting parameters, we solve for the sensitivity coefficients, which in our case represents the ratio of the fractional change in the calculated thermal conductivity to the fractional perturbation in the fitting parameter's value. The sensitivity coefficient is derived by probing the change in derived thermal conductivity as one fitting parameter varies while all other fitting parameters being fixed at their best fit values. Based on the relative changes of the thermal conductivity and the respective fitting parameter, the sensitivity coefficient, S_α, can be defined as[4,5]

$$S_\alpha = \frac{\partial lnk}{\partial ln\alpha} \ ,$$

where k is the calculated thermal conductivity from the Debye-Callaway model and α is the fitting parameter in the model, such as A, B, C and ω_0. We plot the obtained sensitivity coefficients S_A, S_B, S_C and S_{ω_0} for the orthorhombic phase $MAPbI_3$ in Figure S6. The results in Figure S6 indicate that S_B and S_C are distinct with very different values and temperature dependence. S_A and S_{ω_0}, while having similar magnitudes, are of different temperature dependence, which suggests that these two fitting parameters are also unique.

Table S1: Debye-Callaway modelling parameters for the three kinds of perovskite nanowires.

	Phase	θ (K)	v (ms^{-1})	d (nm)	A (10^{-40} s^3)	B (10^{-17} sK^{-1})	C (10^{11} s^{-1})	ω_0 (10^{12} $rads^{-1}$)
$MAPbI_3$	orthorhombic	141	1653	460	1.3	7.95	1.76	3.56
	tetragonal	131	1480	460	15.7	0.84		
$MAPbBr_3$	orthorhombic	214	2276	290	0.82	0.31	3.41	6.85
	tetragonal	160	1744	290	6.44	0.52		
	cubic	219	1896	290	5.9	0.57		
$CsPbBr_3$	orthorhombic	224	1577	390	3.3	2.7		

Note 2: Probing minimum thermal conductivity in perovskites

We follow the method developed by Cahill et al.[6] to calculate the minimum thermal conductivity.

To calculate minimum thermal conductivity of $CH_3NH_3PbI_3$, we use the following equation,

$$k_{min} = (\frac{\pi}{6})^{\frac{1}{3}} k_B n^{\frac{2}{3}} \sum_i v_i (\frac{T}{\theta_i})^2 \int_0^{\theta_i/T} \frac{x^3 e^x}{(e^x - 1)^2} dx,$$

where n is the number density of atoms, v_i is the speed of sound, and $\theta_i = v_i(\frac{\hbar}{k_B})(6\pi^2 n)^{\frac{1}{3}}$. We used $v_l = 2135\, m/s$, $v_t = 1087\, m/s$, and $v_m = 1218\, m/s$ from the literature[1], which yield k_{min} of about 0.11 $Wm^{-1}K^{-1}$ at 300 K.

Note 3: Evaluation of the thermal contact resistance

The total measured thermal resistance (R_{tot}) in the micro-bridge measurement scheme can be expressed as $R_{tot} = R_s + R_{c1} + R_{c2}$, where R_s is the thermal resistance of the sample, R_{c1} and R_{c2} are the thermal resistance of the contacts between the nanowire and Pt electrodes on the two membranes. In order to evaluate the effect of contact resistance, we follow the analysis of contact resistance[7] between a nanobeam and suspended membranes and express the thermal contact resistance as $R_c = \frac{1}{4} \cdot \frac{1}{\sqrt{hPkA_c}\tanh\left(\sqrt{\frac{hP}{kA_c}}L_c\right)}$, where h is the heat transfer coefficient between the nanowire and supported Pt electrode, P is the effective lateral width of the contact, A_c is the cross-sectional area of the nanowire and k is the estimated intrinsic thermal conductivity of the measured samples. Among the above parameters, $h = {k_I}/{l_I}$ is critical, where k_I and l_I represent interface conductivity and interface length, respectively. We confirm an intimate contact by 45-degree tilt SEM image (Figure S1) and therefore ensure a short interface length. We estimate the interface length to be less than 30 nm. In addition, we use organometallic Pt to increase the contact area between sample and membranes and to fill in any gaps at the interface. We conservatively estimate the interface conductivity with a lower limit of 1 $Wm^{-1}K^{-1}$. The estimated intrinsic thermal conductivity of the measured nanowire sample is extracted from the literature of bulk $CH_3NH_3PbI_3$ sample. With other geometry parameters confirmed, for example, R_c and R_{tot} are$3.6 \times 10^6\ WK^{-1}$ and $7.1 \times 10^7\ WK^{-1}$, respectively, at 290 K for the $CH_3NH_3PbI_3$ sample shown in Figure 2. Finally, we can estimate that thermal contact resistance account for about 5% of total resistance in our measurement (Figure 2b).

References:

1. Feng, J. Mechanical properties of hybrid organic-inorganic $CH_3NH_3BX_3$ (B = Sn, Pb; X = Br, I) perovskites for solar cell absorbers. *APL Materials* **2014,** 2 (8), 081801.

2. Hirotsu, S.; Suzuki, T.; Sawada, S. Ultrasonic Velocity around the Successive Phase Transition Points of $CsPbBr_3$. *J. Phys. Soc. Jpn.* **1977,** *43*, 575-582.

3. Lee, W.; Li, H.; Wong, A. B.; Zhang, D.; Lai, M.; Yu, Y.; Kong, Q.; Lin, E.; Urban, J. J.; Grossman, J. C.; Yang, P. Ultralow Thermal Conductivity in All-Inorganic Halide Perovskites. *Proc. Natl. Acad. Sci. U S A* **2017,** *114* (33), 8693-8697.

4. Koh, Y. K.; Singer, S. L.; Kim, W.; Zide, J. M. O.; Lu, H.; Cahill, D. G.; Majumdar, A.; Gossard, A. C. Comparison of the 3ω Method and Time-Domain Thermoreflectance for Measurements of the Cross-Plane Thermal Conductivity of Epitaxial Semiconductors. *J. Appl. Phys.* **2009**, *105* (5), 054303.

5. Kimling, J.; Philippi-Kobs, A.; Jacobsohn, J.; Oepen, H. P.; Cahill, D. G. Thermal conductance of interfaces with amorphous SiO_2 measured by time-resolved magneto-optic Kerr-effect thermometry *Phys. Rev. B* **2017**, *95*, 184305.

6. Cahill, D. G.; Watson, S. K.; Pohl, R. O. *Phys. Rev. B* Lower Limit to the Thermal Conductivity of Disordered Crystals. **1992,** *46* (10), 6131-6140.

7. Zhu, J.; Hippalgaonkar, K.; Shen, S.; Wang, K.; Abate, Y.; Lee, S.; Wu, J.; Yin, X.; Majumdar, A.; Zhang, X. Temperature-gated thermal rectifier for active heat flow control. *Nano Lett.* **2014,** *14* (8), 4867-72.